Effect of void shape and highly conducting boundary on the 2D conductivity of porous materials

Tung Doan, Hung Le-Quang, Quy-Dong To

Effect of void shape and highly conducting boundary on the 2D conductivity of porous materials

Tung Doan[a,b], Hung Le-Quang[*a,], Quy-Dong To[a,*]

[a]Université Paris-Est, Laboratoire Modélisation et Simulation Multi Echelle, MSME
UMR 8208 CNRS, 5 Boulevard Descartes, 77454 Marne-la-Vallée Cedex 2, France
[b]National University of Civil Engineering, No. 55 Giai Phong street, Hai Ba Trung
District, Hanoi, Vietnam

Abstract

In this paper, the heat conductivity of two-dimensional (2D) material containing arbitrary shape pore with highly conducting pore boundary are considered. To model the distinct heat transfer behavior of the pore boundary, the line conduction model is used. The heterogeneity problem of a single void embedded in an infinite matrix is then investigated and solved with the complex variable and the Conformal Mapping techniques. The results of the latter are then used to obtain the effective heat conductivity of the porous material with different homogenization schemes.

Keywords: Heat conductivity, Numerical conformal mapping, 2D heat transfer, Eshelby problem, arbitrary shape void, surface effect

1. Introduction

Two dimensional thermal properties of materials containing defects or inclusions have been predicted, analytically or numerically, by numerous methods. Analytical solutions can be obtained for simple regular shape of defects close to circular and elliptical (Stroh, 1958; Florence and Goodier, 1959; Gao

---

[*]Corresponding authors. E-mail address: quang-hung.le@u-pem.fr, quy-dong.to@u-pem.fr.

et al., 2002; Zhang and Wang, 2016). However, for more complex shapes in the general cases, numerical methods are available. For 2D materials, one of the popular numerical techniques that has been used widely is the combination of complex variable method and Conformal Mapping (CM) method (Chen, 1967; Hasebe and Inohara, 1980; Hasebe et al., 1988; Hasebe and Chen, 1996; Chao and Shen, 1998; Qin, 2000; Vinh et al., 2005; Jafari and Mohammad , 2019).

Regarding the inhomogeneity problems, one of the major concerns is the interface/surface effects. For materials with vacancies, the void boundary conductivity can be modified due to the environment, for example the presence of water-vapour and moisture (Ben-Da Yan et al., 1987; Awakuni and Calderwood, 1972; Boyle and Jones, 1977) or oxydation processes (Cox et al., 1988). The conductivity can also be enhanced intentionally by surface engineering techniques (Williams and Jackman, 2003). Within the scope of this paper, we aim to study the thermal properties of 2D material, which consist voids with arbitrary shapes and with the effects of surface conductivity taken into account. Following Hashin (2001); Benveniste (2006), the imperfect interface model will be used by considering the surface effect as a very thin layer of material of zero thickness (Huy and Sánchez-Palencia, 1974). To our best knowledge, there has been no study using this approach. The method provided by the present work can be adopted to other physically transport problems, such as electric conduction, magnetism, etc.

The paper will be organized as follows. First, we describe the general thermal problem statement for the homogenization for 2D porous materials, without and with surface effects (Sec. 2). Next, we briefly explain the complex variable method and Numerical Conformal Mapping techniques and using them to solve the thermal problem of plate with a single arbitrary void with surface effects under uniaxial heat flux at infinity (Sec. 3). In Sec. 4, we check

the accuracy of the proposed method using analytical solution as well as final element model. Then, the results from Sec. 3 are used to predict the thermal properties using standard homogenization schemes including dilute and MT estimation schemes. Finally, some concluding remarks are given in the last section.

As for notations, we use normal characters for scalars, bold characters for vectors or tensors. Regarding tensor operators, $\cdot$ stands for inner product, $:$ for double inner product.

2. Homogenization framework for 2D materials

2.1. General problem description

In the present work, we consider a 2D heterogeneous material consisting of n inclusion phases $1, 2, ..., n$ which are assumed to be randomly embedded in a matrix phase (see Fig. 1). The matrix, denoted as phase 0, and the i-th inclusion, which is supposed to be individually homogeneous, is referred to as phase i with $i = 1, 2, ..., n$. We denote by Ω the 2D domain occupied by a Representative Elementary Area (REA) of the heterogeneous material considered. The external boundary and the area of Ω are designated by $\partial\Omega$ and $|\Omega|$, respectively. Similarly, the subdomain occupied by i-th phase and its area are symbolized by Ω_i and $|\Omega_i|$. The interface between the matrix Ω_0 and the i-th inclusion Ω_i is a closed curve denoted by Γ_i. On each interface Γ_i, the arc coordinate s runs in the counterclockwise direction with the inclusion always lying on the left and the matrix on the right. Consequently, the normal unit vector $\mathbf{n}$ is directed inwards and the heat flux jump across the interface Γ_i becomes $[\![\boldsymbol{q}]\!] = \boldsymbol{q}^{(0)} - \boldsymbol{q}^{(i)}$. For later use, the opposite vector of $\mathbf{n}$ is called $\mathbf{m}$ ($\mathbf{m} = -\mathbf{n}$), directed in outward directions. We note that for ideal interface the normal components of the heat flux jump is expected to be vanished $[\![\boldsymbol{q}]\!].\mathbf{n} = 0$. This is not the case for the conducting interface whose flux contribution is not negligible. The detailed behavior of the interface will

be presented in the later section.

At micro-scale, in each phase i, the heat flux vector $\boldsymbol{q}$ is related to the infinitesimal intensity field $\boldsymbol{e}$ by the following equation:

$$\boldsymbol{q}(\mathbf{x}) = \boldsymbol{K}^{(i)} \cdot \boldsymbol{e}(\mathbf{x}), \quad \boldsymbol{e}(\mathbf{x}) = -\nabla T(\mathbf{x}) \tag{1}$$

where $\mathbf{x}$ is the position vector belong to phase i $(= 0, 1, 2, ..., n)$ and $\boldsymbol{K}^{(i)}$ denotes the second-order conductivity tensor of phase i and T the temperature. In case the i-th heterogeneity is a pore inclusion, the thermal conductivity tensors $\boldsymbol{K}^{(i)}$ will vanish, i.e. $\boldsymbol{K}^{(i)} = 0$.
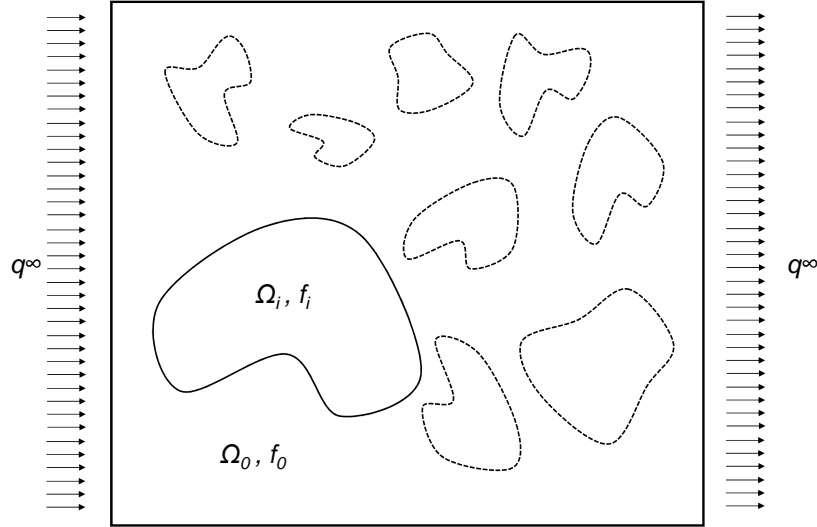

Figure 1: A 2D material containing inclusions of arbitrary shape.

At macroscopic scale, since the inclusions are supposed to be distributed

randomly in the matrix, the heterogeneous material under investigation is assumed to be statistically homogeneous. Due to the linear property of the local constitutive laws of each phase and the interface/surface conditions, the corresponding effective thermal behavior law remains linear and can be written as follows:

$$\mathbf{Q} = \boldsymbol{K}^e \cdot \mathbf{E}, \tag{2}$$

where $\mathbf{Q}$ and $\mathbf{E}$ are respectively the overall heat flux and intensity field vector and $\boldsymbol{K}^e$ is the second-order thermal conductivity tensor which will be estimated in the present work.

2.2. Thermal conductive interface model

For later use, we define the tangential unit vector along s as $\mathbf{l}$ and the normal unit vector obtained by rotating the latter in the counter clockwise direction as $\mathbf{n}$ (Fig. 2). On the non ideal conducting interface, there is the heat flux $\boldsymbol{\tau}$ flows along the tangential direction $\boldsymbol{l}$ and $\boldsymbol{\tau} = \tau\boldsymbol{l}$. The energy conservation equation for a line of dimension ds presents in the form:

$$q_n = [\![\boldsymbol{q}]\!] \cdot \boldsymbol{n} = \frac{d\tau}{ds}. \tag{3}$$

In above equation, $[\![\boldsymbol{q}]\!] \cdot \mathbf{n}$ denotes the jump of the heat flux vector across the surface Γ; τ is the heat flow within the wire, and q_n represents the normal heat flux. The notation $\mathrm{d}(\bullet)/\mathrm{d}s$ measures the variation of quantity $\bullet$ along the interface/surface with respect to the variable s. Within the wire, we assume that the conduction is of Fourier type

$$\tau = -k_s \frac{dT}{ds}, \tag{4}$$

with k_s being the conductivity. Combined with the Eq (3) we obtain
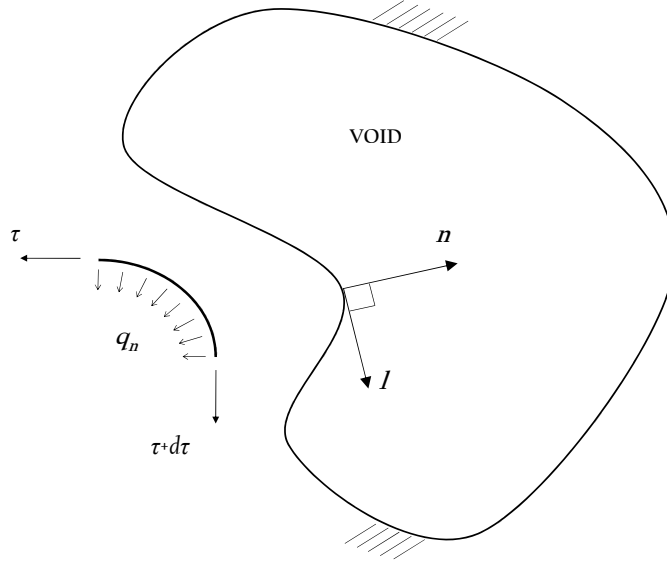
$$q_n = -k_s \frac{d^2T}{ds^2}. \tag{5}$$

5

Figure 2: Analysis of line thermal

2.3. Thermal homogenization for 2D materials with surface effects

Since the temperature T is continuous across the interface/surface Γ_i, the macroscopic intensity field defined by Eq. (2) is exactly equal to the area average intensity field over Ω, i.e.

$$\mathbf{E} = \sum_{i=0}^{n} f_i \langle \boldsymbol{e} \rangle_i, \tag{6}$$

where $\langle \bullet \rangle_i$ denotes hereafter the area average of $\bullet$ over Ω_i and $f_i = |\Omega_i|/|\Omega|$ designates as the area fraction of i-th phase. On the other hand, due to the discontinuity of the heat flux tensor across the interface/surface Γ_i, the macroscopic heat flux tensor provided by Eq.(2) is not simply the area average of the local counterpart $\boldsymbol{q}(\mathbf{x})$. More precisely, starting from the diver-

6

gence theorem, the macroscopic heat flux $\mathbf{Q}$ reads

$$\mathbf{Q} \;=\; \sum_{i=0}^{n} f_i \langle \boldsymbol{q} \rangle_i - \sum_{i=1}^{n} f_i \frac{1}{|\Omega_i|} \int_{\Gamma_i} (\llbracket \boldsymbol{q} \rrbracket . \boldsymbol{n}) \mathbf{x} \, \mathrm{d}s. \tag{7}$$

Based on (3) and using the facts that the integral on the closed curve vanish $\int_{\Gamma_i} \mathrm{d}(\tau \mathbf{x}) = 0$ and $\frac{\mathrm{d}\mathbf{x}}{\mathrm{d}s} = \mathbf{l}$, the integrals on Γ_i can be further simplified by

$$\int_{\Gamma_i} (q_n \cdot \mathbf{x}) \mathrm{d}s = - \int_{\Gamma_i} \tau \mathbf{l} \mathrm{d}s. \tag{8}$$

As a result, the overall heat flux can be recast in the form

$$\mathbf{Q} \;=\; \sum_{i=0}^{n} f_i \langle \boldsymbol{q} \rangle_i + \sum_{i=1}^{n} f_i \frac{1}{|\Omega_i|} \int_{\Gamma_i} \tau \mathbf{l} \mathrm{d}s. \tag{9}$$

Next, the thermal conductivity tensor $\boldsymbol{K}^{si}$ of the interface/surface Γ_i and the localization tensor of the i-th inclusion $\boldsymbol{L}^i$, can be defined as follows:

$$\langle e \rangle_i = \boldsymbol{L}^i \cdot \mathbf{E}, \quad \langle \boldsymbol{q} \rangle_{\Gamma_i} = \boldsymbol{K}^{si} \cdot \langle e \rangle_i, \tag{10}$$

where $\langle \boldsymbol{q} \rangle_{\Gamma_i}$ represents the line average of flux over the interface/surface Γ_i and takes the form

$$\langle \boldsymbol{q} \rangle_{\Gamma_i} \;=\; \frac{1}{|\Omega_i|} \int_{\Gamma_i} (\tau \mathbf{l}) \mathrm{d}s. \tag{11}$$

In case the phase i is a pore, the area average of intensity field $\langle e \rangle_i$ is determined by

$$\langle e \rangle_i \;=\; -\frac{1}{|\Omega_i|} \int_{\Gamma_i} (T \mathbf{m}) \mathrm{d}s. \tag{12}$$

From Eqs. (9) and (10) we obtain

$$\mathbf{Q} = \left\{ \boldsymbol{K}^0 + \sum_1^n f_i(\boldsymbol{K}^i + \boldsymbol{K}^{si} - \boldsymbol{K}^0) \cdot \boldsymbol{L}^i \right\} \cdot \mathbf{E}. \tag{13}$$

From Eqs. (2) and (13), the effective conductivity tensor can be determined by

$$\boldsymbol{K}^e = \boldsymbol{K}^0 + \sum_1^n f_i(\boldsymbol{K}^i + \boldsymbol{K}^{si} - \boldsymbol{K}^0) \cdot \boldsymbol{L}^i. \tag{14}$$

In general, for 2D problem consisting of more than one inclusion, it is impossible to find the exact solution for $\boldsymbol{K}^{si}$ and $\boldsymbol{L}^i$ analytically. In this situation, either numerical methods are applied to calculate exactly these tensors or some approximate approaches based on micromechanical schemes must be used to estimate the values. Both approaches need to solve separately the Eshelby or heterogeneity problems, in which an infinite plate containing single inclusion subject to constant uniform heat flux at infinity. The results of these problems can be used to estimate the localization tensor $\boldsymbol{L}^i$ and the conductivity tensor $\boldsymbol{K}^{si}$.

Next, our subject are the estimations of the effective conductivity tensor, by dilute and MT schemes:

$$\begin{aligned}
\boldsymbol{K}^e_{\mathrm{Dilute}} &= \boldsymbol{K}^0 + \sum_1^n f_i(\boldsymbol{K}^i + \boldsymbol{K}^{si} - \boldsymbol{K}^0) \cdot \boldsymbol{L}^i, \\
\boldsymbol{K}^e_{\mathrm{MT}} &= \{f_0 \boldsymbol{K}^0 + \sum_1^n f_i(\boldsymbol{K}^i + \boldsymbol{K}^{si}) \cdot \boldsymbol{L}^i\} \cdot \{f_0 \boldsymbol{I} + \sum_1^n f_i \boldsymbol{L}^i\}^{-1}. \quad (15)
\end{aligned}$$

In special case where there is only one species of nanovoid with the area fraction f, the two foregoing estimates read

$$\boldsymbol{K}^e_{\text{Dilute}} = \boldsymbol{K}^0 + f(\boldsymbol{K}^{s1} - \boldsymbol{K}^0) \cdot \boldsymbol{L}^1,$$

$$\boldsymbol{K}^e_{\text{MT}} = \left\{(1-f)\boldsymbol{K}^0 + f\boldsymbol{K}^{s1} \cdot \boldsymbol{L}^1\right\} \cdot \left\{(1-f)\boldsymbol{I} + f\boldsymbol{L}^1\right\}^{-1}. \quad (16)$$

In following sections, we will step by step explain solution to the heterogeneity problem of a 2D plate with a single void, subjected to constant uniform heat flux at infinity. We also assume the the matrix is made of isotropic material of conductivity k_m and the pore boundary of conductivity k_s as before.

3. Solution for problem with single void under uniform heat flux at infinity

3.1. Complex variable and conformal mapping methods

The proposed solution is based on the popular complex variable and conformal mapping methods (Muskhelishvili, 2008). The method for thermal problem will be presented briefly and more details can be found in the Appendix A.

Instead of working in the usual complex plane, i.e variable $z = x + iy$, $i = \sqrt{-1}$ and in the domain exterior to the hole of arbitrary shape with boundary conditions (5), we solve the problem in a transformed plane, variable ζ and inside a unit circle disk $|\zeta| < 1$. In this case, $\zeta = \omega(z)$ is the mapping function depending on the shape of the hole. It is sufficient to find the complex function $\varphi_1(\zeta)$ which generates the complex flux $q = q_x - iq_y$ and temperature field T as follows

$$2T = \varphi_1(\zeta) + \overline{\varphi_1(\zeta)}, \quad (17)$$

$$q = -k_m \frac{\varphi_1'(\zeta)}{\omega'(\zeta)} \quad (18)$$

9

In addition, the expressions of the temperature T and the q must satisfy the boundary conditions (5) written using ζ coordinate. Posing $n = n_x + in_y$, the normal heat flux q_n on the boundary Γ can be computed by

$$q_n = \Re(qn), \tag{19}$$

Next, we need to find the expressions for the vector n and $\frac{\mathrm{d}}{\mathrm{d}s}$ defined on the boundary Γ. From the identities derived in Appendix A, we obtain the results

$$\frac{\mathrm{d}}{\mathrm{d}s}f(\zeta) = -\frac{i\zeta f'(\zeta)}{|\omega'(\zeta)|}, \quad \frac{\mathrm{d}}{\mathrm{d}s}\overline{f(\zeta)} = \frac{i\overline{\zeta}\overline{f'(\zeta)}}{|\omega'(\zeta)|} \quad \forall f(\zeta), \tag{20}$$

and

$$n = \frac{\omega'\zeta}{|\omega'|}. \tag{21}$$

Consequently, the boundary conditions (5) can be expressed explicitly in terms of ζ only and on the unit circle

$$2k_m\Re\left\{\frac{\omega'\zeta}{|\omega'|}\frac{\varphi_1'(\zeta)}{\omega'(\zeta)}\right\} = k_s\frac{\mathrm{d}^2}{\mathrm{d}s^2}(\varphi_1(\zeta) + \overline{\varphi_1(\zeta)}), \quad |\zeta| = 1 \tag{22}$$

and can be used to solve the unknown potential function $\varphi_1(\zeta)$.

3.2. Schwarz-Christoffel mapping functions

The mapping method we use is based on Schwarz-Christoffel (SC) transformation, which is a useful mapping tool can map a unit circle onto the interior of a simple polygon or vice versa by the following mapping function

$$\omega(\zeta) = C\int_{w_1}^{\zeta}\prod_{k=1}^{N}\left(1 - \frac{w}{w_k}\right)^{1-\beta_k}\frac{1}{w^2}dw + A, \tag{23}$$

where N is the number of the sides of the polygon, $\beta_k \pi$ are the interior angles of the polygon verifying $\sum_{k=1}^{N} \beta_k = N - 2$, w_k is the prevertices of the image of the polygon in the canonical plane, C is multiplicative constant, relate to the rotation and dilation of the mapping, and A is a constant relating to the location of the image around the complex plane.

In general, for regular polygons, this integral can be solved analytically (Neuber, 1962). However, for general cases, the integral must be evaluated numerically by using Taylor series expansion. At $\zeta = 0$, to the order of expansion O^M, the integrand can be expanded as

$$\prod_{k=1}^{N} \left(1 - \frac{w}{w_k}\right)^{1-\beta_k} \frac{1}{w^2} \cong \sum_{j=-2}^{O^M} a_j w^j. \tag{24}$$

The term a_{-1} is set to zero to satisfy the single valuedness of the transformation. We also remark that due to the smooth approximation, the void shape will be rounded at the corners of the polygons.

This integrand is calculated by the Matlab SC toolbox developed by Driscoll (1996). Being given coordinates of all vertices of a void (polygon), this toolbox helps to find all necessary CM transformation factors, including the values of β_k, w_k and the multiplicative constant C. By combining Eqs. (23) and (24), the estimation of $\omega(\zeta)$ can be found as an explicit polynomial function of ζ. Further details of how the numerical factors affect the accuracy of the mapping tool will be studied in Section 4.

3.3. Solution for single void in an infinite plate

In this section, we consider the case where a plate with a void is subject to remote uniaxial heat flux q_∞ making an angle χ with axis x. To solve the

problem, we decompose the potential function of the plate in the form

$$\varphi_1(\zeta) = \varphi_2(\zeta) + \varphi_3(\zeta), \tag{25}$$

where $\varphi_2(\zeta)$ is the potential function of a plate without the void under uniform heat flux, of which the solution is already available

$$\varphi_2(\zeta) = -\frac{q_\infty}{k} e^{-i\chi} \omega(\zeta), \tag{26}$$

and $\varphi_3(\zeta)$ is the additional potential function account for the temperature field caused by the void. The latter can be expanded by using Taylor series:

$$\varphi_3(\zeta) = \sum_{n=0}^{O^s} \alpha_n \zeta^n \tag{27}$$

with O^S being the order of expansion of the potential function.

To find $\varphi_3(\zeta)$, which are now the constraints on the unit circle $|\zeta| = 1$, the collocation method with discrete points on the unit circle is employed to compute the coefficients α_n. The governing equations are solved for both real and imaginary parts leading to a system of linear equations with the real and imaginary parts of α_n as unknowns. After solving the potential function in form of Taylor series, the temperature and heat flux are calculated for a set of points on the surface boundary. The average intensity field and heat flux tensors of the thermal void are then numerically integrated based on Eqs. (11)-(12).

For comparison purpose, we present the analytical solution for the case of circular void, as a base to compare with the CM method. Assuming that the circle void has the radius R located at the origin of the polar coordinate system (r, θ). The plate, subject to heat flux q_∞ at infinity along horizontal direction, has the edge conductivity and matrix conductivity are k_s and k_m

correspondingly. Based on the symmetry/anti-symmetry of this case, we are looking for solution in the form

$$T = -f(r) \cos \theta. \tag{28}$$

in the polar coordinate system (r, θ). To satisfy the Laplace equation, T must admit the form

$$f = Ar + B/r, \tag{29}$$

where A, B are unknown constants to be determined by using boundary conditions. The heat flux components in the polar coordinate system takes the forms

$$q_r = k_m f'(r) \cos \theta = k_m(A - B/r^2) \cos \theta, \tag{30}$$

$$q_\theta = k_m \frac{f(r)}{r} \sin \theta = k_m(A + B/r^2) \sin \theta. \tag{31}$$

By solving the boundary conditions at infinity and at the hole boundary, we have

$$A = q_\infty/k_m, \quad B = \frac{q_\infty}{k_m} \frac{(Rk_m - k_s)}{(Rk_m + k_s)} R^2. \tag{32}$$

13

Then, we obtain the final solutions

$$q_r = q_\infty \left[1 - \left(\frac{Rk_m - k_s}{Rk_m + k_s} \right) \left(\frac{R}{r} \right)^2 \right] \cos\theta, \tag{33}$$

$$q_\theta = q_\infty \left[1 + \left(\frac{Rk_m - k_s}{Rk_m + k_s} \right) \left(\frac{R}{r} \right)^2 \right] \sin\theta, \tag{34}$$

$$T = -r \frac{q_\infty}{k_m} \left[1 + \left(\frac{Rk_m - k_s}{Rk_m + k_s} \right) \left(\frac{R}{r} \right)^2 \right] \cos\theta, \tag{35}$$

$$\tau = r \frac{q_\infty k_s}{Rk_m} \left[1 + \left(\frac{Rk_m - k_s}{Rk_m + k_s} \right) \left(\frac{R}{r} \right)^2 \right] \sin\theta. \tag{36}$$

In case $k_s = 0$, $B = \dfrac{q_\infty}{k_m} R^2$, we recover the classical solution without the boundary effect

$$q_r = q_\infty \left[1 - \left(\frac{R}{r} \right)^2 \right] \cos\theta, \tag{37}$$

$$q_\theta = q_\infty \left[1 + \left(\frac{R}{r} \right)^2 \right] \sin\theta, \tag{38}$$

$$T = -r \frac{q_\infty}{k_m} \left[1 + \left(\frac{R}{r} \right)^2 \right] \cos\theta. \tag{39}$$

It is noted that at the hole boundary, where $r = R$, q_r vanishes as expected.

4. Numerical examples

4.1. Infinite plate with single void under uniform heat flux at infinity

In this section, we compute and compare the results obtained by the CM method and COMSOL Multiphysics®, a standard Finite Element Method (FEM) code for single void problems. In the FEM model, we use a square domain with sufficiently large dimensions and model the surface thermal effect as a thin band of material of thickness h and conductivity $\tilde{k}_s = k_s/h$.

14

Numerical experiences show that when the size ratio of plate-to-void is of order 30 : 1 and the ratio edge layer thickness to the characteristic size of the polygonal void is about 1/2000, we obtain satisfactory results.

First, let us look into the CM solution to the circular void problem where analytical solution is available from previous section. Without loss of generality, we assume $q_\infty = 1$, $k_m = 1$, $k_s = 10$, $R = 1$ and the flux direction angle $\chi = 0$. The analytical solution at the boundary of the circular void $(r = R)$ gives

$$
\begin{aligned}
q_r &= \frac{20}{11}\cos\theta, \\
q_\theta &= \frac{2}{11}\sin\theta, \\
T &= -\frac{2}{11}\cos\theta, \\
\langle q_{11}\rangle^i &= \frac{20}{11}.
\end{aligned}
$$

If the surface thermal effect is neglected, i.e. $k_s = 0$, the corresponding results are

$$
\begin{aligned}
q_\theta &= 2\sin\theta, \\
T &= -2\cos\theta.
\end{aligned}
$$

Regarding the CM method, the exact transformation function for the circle is $\omega(\zeta) = 1/\zeta$. Using SC transformation, the circle is approximated by a N-side equilateral polygon. The results of numerical mapping function for different values of N show that accuracy can be achieved with $N = 80$, $\omega(\zeta) = 0.999/\zeta + 0.001$.

The accuracy of the CM method is accessed by the temperature at two key points on the void boundary (see Fig. 3 for illustration), as well as the

15

inclusion average heat flux and intensity field under horizontal heat flux condition. First, the results for circular void alone are reported in Table 1. It can be seen that there is virtually no difference between the analytical solution and FEM. The relative difference between the CM method and the others is negligible (0.2%). This excellent agreement also confirms the accuracy of the CM method as well as the FEM model, allowing us to continue with non-circular voids including ellipse, rectangle and arbitrary shape (Fig. 4). The detailed dimension of all the holes using in this paper can be found in Appendix B. The temperature values at some key locations are given in Table 2.

Finally, we investigate the inclusion averages of heat flux and intensity field, the two important quantities that affect directly on the effective properties when using homogenization schemes. Table 3 shows that the inclusion average heat flux $\langle q_{11} \rangle^i$ and average intensity field $\langle e_{11} \rangle^i$ are in excellent agreement. The relative differences between the two methods for all shapes are less than 5%.
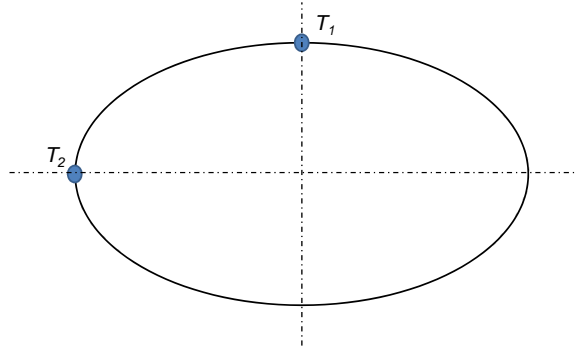

Figure 3: A sketch of double symmetric void of arbitrary shape. Void boundary temperature at the intersections with symmetry axes are chosen for comparisons

16

Method	$k_s = 0$		$k_s = 10$		
	T_1	T_2	T_1	T_2	$\langle q_{11} \rangle^i$
Analytic	0.000	2.000	0.000	0.1818	1.818
FEM	0.000	2.000	0.000	0.1817	1.818
CM	0.000	1.997	0.000	0.1815	1.867

Table 1: Temperature and inclusion average heat flux of the circular void at the boundary, with and without surface thermal effect
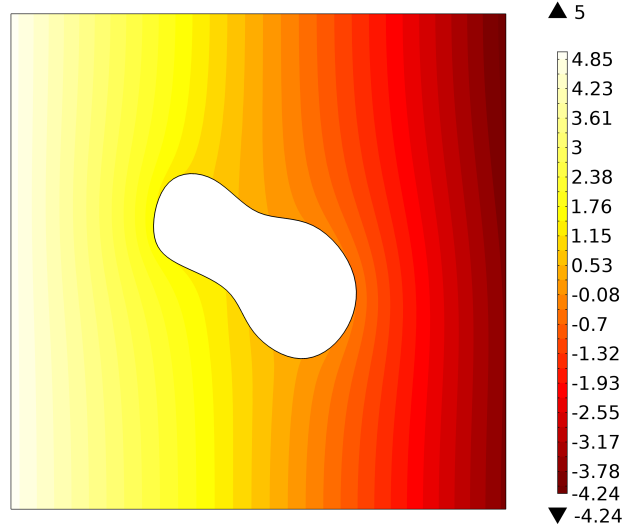

Figure 4: Temperature contour of void with arbitrary shape under horizontal heat flux.

4.2. Effective conductivity for the case of randomly distributed pores

Solutions from previous subsections are used to estimate thermal properties of materials based on the Dilute and MT schemes (Eq. 15). The latter will be compared with results issued from the FEM method. Within the framework of this work, we only consider FEM models containing identical voids whose location and orientation are distributed randomly (Fig. 5). To ensure the statistical convergence, we carry out computations on 30 independent samples each of which contains 20 voids. Meanwhile, in the NCM

		NCM		FEM	
Shape		T_1	T_2	T_1	T_2
Ellipse	⬭	0.000	0.435	0.000	0.447
Square	◻	0.000	0.249	0.000	0.259
Octagon	⬡	0.000	0.172	0.000	0.172

Table 2: Comparison of boundary temperature values for different void shape with $k_s = 10$.

		NCM		FEM	
Shape		$\langle q_{11}\rangle^i$	$\langle e_{11}\rangle^i$	$\langle q_{11}\rangle^i$	$\langle e_{11}\rangle^i$
Circle	◯	1.867	0.185	1.818	0.182
Ellipse	⬭	2.598	0.232	2.526	0.232
Square	◻	1.849	0.229	1.933	0.238
Octagon	⬡	1.913	0.184	1.839	0.179
arbitrary	⬠	2.174	0.335	2.120	0.330

Table 3: Comparison of inclusion average heat flux and intensity field tensor elements for various nanovoid shape with $k_s = 10$.

methods, the average stiffness tensor $\boldsymbol{K}^{si}$ and the localization tensor $\boldsymbol{L}^i$ of each inclusion with different orientation χ_i are calculated by taking rotation transformations of an angle χ_i from the original solution $\boldsymbol{K}^{s1}$ and $\boldsymbol{L}^1$ with original direction $\chi_1(=0)$.

The results for circular and other shapes are shown in Fig. 6 and Fig. 7. From the results of circular void, it can be seen that our MT model result match well with that of Le-Quang et al. (2010). However, in comparison with FEM model, the MT results only fit well at a small range of area fraction. At higher fractions, say $f > 0.1$, Self-Consistent predictions seem to be a better choice, based on circular void results.

5. Conclusions

In this work, we study the problem of determining the thermal conductivity of 2D materials containing voids of arbitrary shape with surface effects. By first solving the problem involving a single void we then were able to esti-
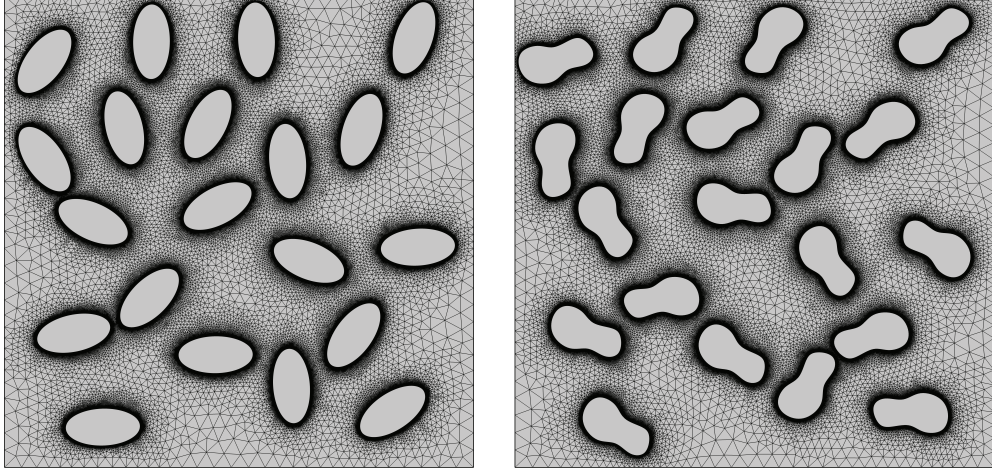
Figure 5: FEM meshing layout for elliptical and arbitrary voids

mate properties of random materials by applying the Dilute and MT schemes.

The single void solution produced by the approach is in excellent agreement with both available analytical solutions and the FEM method for different kinds of shapes, including the arbitrary one. Our investigation shows that MT and dilute estimations, on the other hand, are only accurate within a certain range of area fraction ($f < 0.1$ in the case of our input data).

The results issued from this work are expected to have significant application in science materials, in particular 2D nano materials, e.g. graphene, silicene, etc. A similar procedure can also be easily transformed to electrical conduction, magnetism, diffusion or any other physically analogous transport problems of 2D materials with surface effects. These perspectives will be investigated in future work.
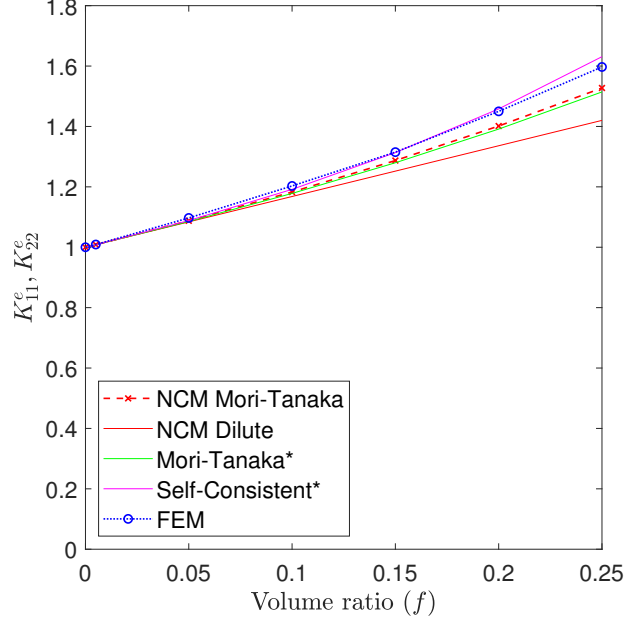
19

Figure 6: Comparison among Dilute, MT, Self-consistent estimates and FEM methods for circular voids (* Results from Le-Quang et al. (2010)).

Appendix A. Expressions in transformed coordinates

For heat transfer problem, the temperature T must satisfy the Laplace equation

$$\nabla^2 T = 0, \tag{A.1}$$

In the conventional complex plane where $z = x + iy$, the Laplace operator is equivalent to

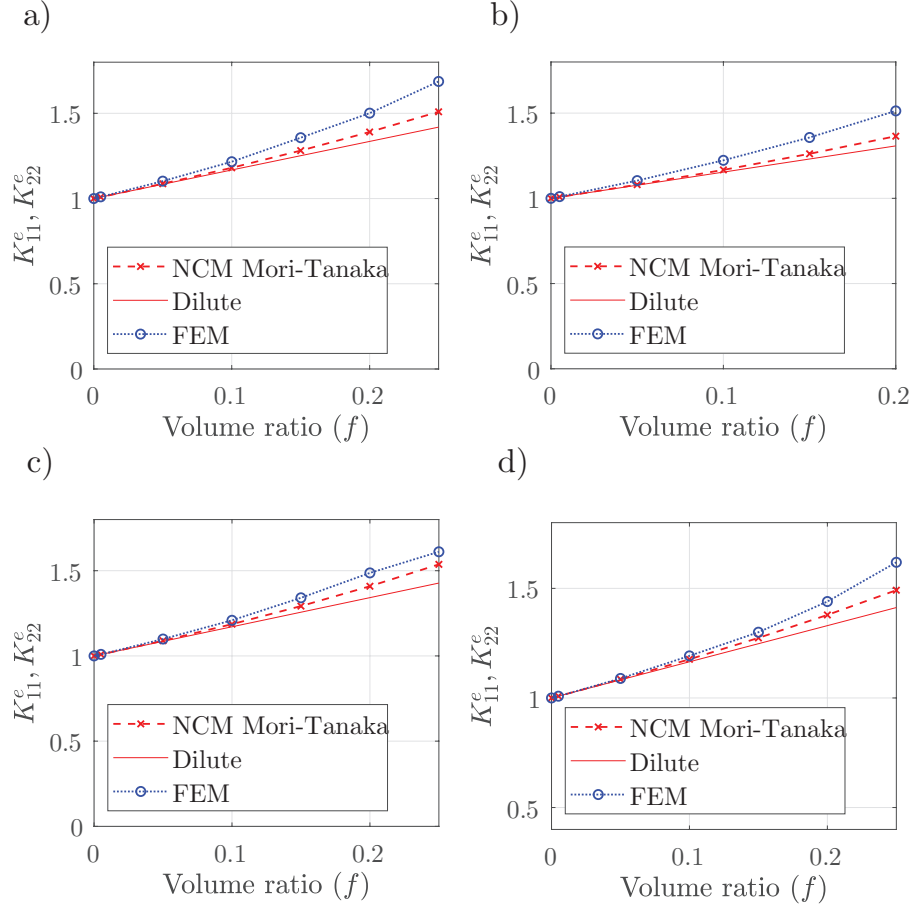$$\nabla^2 = 4\frac{\partial^2}{\partial z \partial \bar{z}} \tag{A.2}$$

Figure 7: Comparison among Dilute, MT estimates and FEM methods for different shapes of voids (a. Ellipse, b. Square, c. Octagon, d. Arbitrary).

After integrating, we must have the relation

$$T = \Re\{\varphi(z)\} = \frac{1}{2}(\varphi(z) + \overline{\varphi(z)}) \tag{A.3}$$

where $\varphi(z)$ is an analytical function of z. The heat flux q with conductivity k_m can be expressed by

$$q_x = -\frac{k_m}{2}[\varphi'(z) + \overline{\varphi'(z)}], \quad q_y = -i\frac{k_m}{2}[\varphi'(z) - \overline{\varphi'(z)}]. \tag{A.4}$$

Next, by introducing the new variable ζ and by using the transformation $z = \omega(\zeta)$, the function $\varphi(z)$ becomes

$$\varphi(z) = \varphi(\omega(\zeta)) = \varphi_1(\zeta). \tag{A.5}$$

In general, the mapping function $z = \omega(\zeta)$ is chosen to map a void plate with boundary Γ in z plane into the unit disk in ζ plane ($|\zeta| \leq 1$) and solve the problem with ζ as variable.

On the unit circle mapped from Γ, we pose $\zeta = e^{-i\theta}$ with θ running from 0 to 2π. This parameterization also guarantees the arc coordinate s on Γ goes in the positive (counter-clockwise) direction. Differential calculus yields the following result

$$d\zeta = -ie^{-i\theta}d\theta = -i\zeta d\theta, \quad d\bar{\zeta} = ie^{i\theta}d\theta = i\bar{\zeta}d\theta$$
$$dz = \omega'(\zeta)d\zeta = -i\omega'(\zeta)\zeta d\theta, \quad ds = |dz| = |\omega'(\zeta)|d\theta \tag{A.6}$$

We can immediately obtain

$$\frac{d\zeta}{ds} = -\frac{i\zeta}{|\omega'|}, \quad \frac{d\bar{\zeta}}{ds} = \frac{i\bar{\zeta}}{|\omega'|}, \quad \frac{dz}{ds} = \frac{i\omega'}{|\omega'|} \tag{A.7}$$

and hence the three identities of (20,21).

Appendix B. Detailed dimensions of voids

The details dimensions of all the voids are summarized in Fig. B.8 where L is the basic dimension and for arbitrary shape, L1=4.6L and L2=2.5L. All the results are to the value of L.
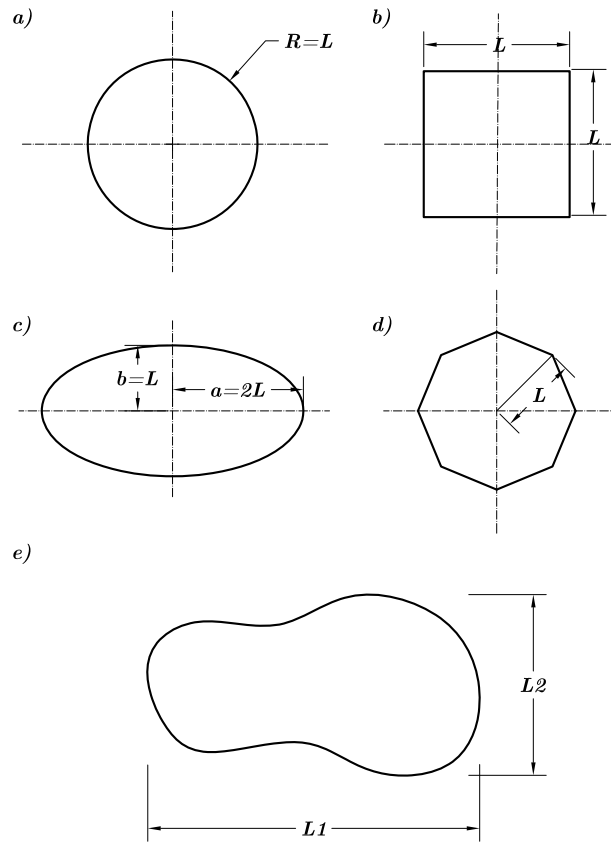
Figure B.8: Void dimensions (a-Circle, b-Square, c-Ellipse, d-Octagon, f-arbitrary)

References

Awakuni, Y., Calderwood, J.H., 1972. Water vapour adsorption and surface conductivity in solids. J. Phys. D: Appl. Phys. 5, 1038–1045.

Ben-Da Yan, Meilink, S., Warren, G., Wynblatt, P., 1987. Water adsorption and surface conductivity measurements onalpha-alumina substrates. IEEE Trans. Compon. Hybr. Manuf. Tech. 10, 247–251. doi:10.1109/TCHMT.1987.1134727.

Benveniste, Y., 2006. A general interface model for a three-dimensional curved thin anisotropic interphase between two anisotropic media. J. Mech. Phys. Solids 54, 708–734.

Boyle, J.F., Jones, K.A., 1977. The effects of co, water vapor and surface temperature on the conductivity of a sno2 gas sensor. J. Elec. Mat. 6, 717–733.

Chao, C., Shen, M., 1998. Thermal stresses in a generally anisotropic body with an elliptic inclusion subject to uniform heat flow. J. Appl Phys. 65, 51–58.

Chen, W., 1967. Plane thermal stress at an insulated hole under uniform heat flow in an orthotropic medium. J. Appl Phys. 34, 133–136.

Cox, D.F., Fryberger, T.B., Semancik, S., 1988. Oxygen vacancies and defect electronic states on the $sno_2(110)$-11 surface. Phys. Rev. B 38, 2072–2083. doi:10.1103/PhysRevB.38.2072.

Driscoll, T.A., 1996. Algorithm 756: A MATLAB Toolbox for Schwarz-Christoffel Mapping. ACM Trans. Math. Softw. 22, 168–186.

Florence, A., Goodier, J., 1959. Thermal stress at spherical cavities and circular holes in uniform heat flow. J. Appl. Mech 26.

Gao, C.F., Zhao, Y.T., Wang, M.Z., 2002. An exact and explicit treatment of an elliptic hole problem in thermopiezoelectric media. Int. J. Solids. Struct. 39, 2665–2685.

Hasebe, N., Chen, Y., 1996. Stress intensity solutions for the interaction between a hole edge crack and a line crack. Int. J. Fract. 77, 351–366.

Hasebe, N., Inohara, S., 1980. Stress analysis of a semi-infinite plate with an oblique edge crack. Ingenieur-Archiv 49, 51–62.

Hasebe, N., Tomida, A., Nakamura, T., 1988. Thermal stresses of a cracked circular hole due to uniform heat flux. J. Therm. Stresses 11, 381–391.

Hashin, Z., 2001. Thin interphase/imperfect interface in conduction. J. Appl. Phys. 89, 2261–2267.

Huy, H.P., Sánchez-Palencia, E., 1974. Phénomènes de transmission à travers des couches minces de conductivitééélevée. J. Math. Anal. Appl. 47, 284–309.

Jafari, Mohammad, 2019. Thermal stress analysis of orthotropic plate containing a rectangular hole using complex variable method. Eur. J. Mech. A-Solid 73, 212–223.

Le-Quang, H., Bonnet, G., He, Q.C., 2010. Size-dependent eshelby tensor fields and effective conductivity of composites made of anisotropic phases with highly conducting imperfect interfaces. Phys. Rev. B 81, 064203.

Muskhelishvili, N., 2008. Singular integral equations: boundary problems of function theory and their application to mathematical physics. Courier Corporation.

Neuber, H., 1962. G. N. Savin, Stress concentration around holes. XI + 430 S. m. 208 Abb. u. 77 Tafeln. Oxford/London/New York/Paris 1961.

Pergamon Press. Preis geb. 84 s. net. J. Appl. Math. Mech. 42, 265–265. doi:10.1002/zamm.19620420618.

Qin, Q.H., 2000. General solutions for thermopiezoelectrics with various holes under thermal loading. Int. J. Solids. Struct. 37, 5561–5578.

Stroh, A., 1958. Dislocations and cracks in anisotropic elasticity. Philos. Mag. 3, 625–646.

Vinh, P.C., Hasebe, N., Wang, X.F., Saito, T., 2005. Interaction between a cracked hole and a line crack under uniform heat flux. Int. J. Fract. 131, 367–384.

Williams, O.A., Jackman, R.B., 2003. Surface conductivity on hydrogen terminated diamond. Semi. Sci. Tech. 18, S34–S40. doi:10.1088/0268-1242/18/3/305.

Zhang, A., Wang, B., 2016. Explicit solutions of an elliptic hole or a crack problem in thermoelectric materials. Eng. Fract. Mech. 151, 11–21.